Microstructural and Mechanical Evaluations of SAW By Manufactured Granular Basic Bonded Cr, Mo, and Cr-Mo Active Fluxes on ST37 Low Carbon Steel

Mahdi Alishavandi
Sharif University of Technology
Mahdi Mohammadmirzaei
Sharif University of Technology
Mahnam Ebadi
Shiraz University
Amir Hossein Kokabi (Kokabi@sharif.edu)
Sharif University of Technology https://orcid.org/0000-0001-7483-0064

Research Article

Keywords: Submerged arc welding, Unfused flux, Active bonded flux, Acicular ferrite, Inclusion, Slag, Impact test, Fractography

Posted Date: February 12th, 2021

DOI: https://doi.org/10.21203/rs.3.rs-167620/v1

Version of Record: A version of this preprint was published at The International Journal of Advanced Manufacturing Technology on January 20th, 2022. See the published version at https://doi.org/10.1007/s00170-021-08238-1.

Abstract

Bead-on-plate submerged arc welding was conducted on St37 steel by manufactured Cr, Mo, and Cr-Mo active basic fluxes produced via the unfused bonded method. The base metal heat-affected zone and weld metal (WM) microstructures were identified and characterized by optical microscopy and scanning electron microscopy. Then, the ferrite morphologies volume fraction of WMs were measured. Moreover, the chemical analysis of slag and inclusions was evaluated by point scan energy-dispersive X-ray spectroscopy and extensively discussed. Inclusions number density and size and their effects on the formation of AF were also elaborated. Then, the WMs' longitudinal tensile strength and Vickers hardness were measured. Finally, the Charpy V-notch test was conducted to determine the impact toughness; the fracture surfaces were investigated, as well.

Introduction

Submerge arc welding (SAW) is one of the main heterogenous fusion welding processes due to its inherent properties such as high joining and deposition rates, deep weld penetration, high-quality weld surface, thick section welding ability, and automatic mode operation. This process is most commonly used in heavy industries such as shipbuilding, tube and pipe manufacturing, large scale structures, power plants, chemical, and nuclear installations [1–4].

The weld metal's (WM) microstructure and mechanical properties can be controlled by adding various alloying elements such as Mo and Cr into flux and the WM's chemical composition [5, 6]. Active or alloying flux should be prepared by unfused methods like agglomerated or bonded fluxes method rather than a fused method to prevent alloying elements degradation and oxidation [7–10]. One of the most critical factors affecting the fusion zone's (FZ) mechanical properties and microstructure is the WM alloying elements that are dictated by BM and welding wire (WW) chemical composition, heat input, flux characteristics, dilution, and chemical reactions of the slag-WM [11]. Furthermore, the basicity index (BI), which defines as the proportion of basic to acidic compounds of the flux ingredients (such as CaO, SiO_2, TiO_2, Al_2O_3), determines the ability of the flux to protect alloying elements [12].

It is well known that steels' welding relies on the optimum size and number density of nonmetallic inclusions as a potent heterogeneous nucleation site, which promotes acicular ferrite (AF) formation [13–15]. The best impact toughness in steels is achieved through AF due to the high angle grain boundaries (HAGB) density and chaotic fine interlocking sheaves microstructure [16–18]. Mabucci et al. [19] showed that manganese depletion in the ferrite matrix-manganese sulfide interface is associated with manganese precipitates' formation on the oxide inclusions during cooling; this is one of the critical mechanisms of AF formation.

The appropriate size of nonmetallic inclusions for AF nucleation stated in the literature is 1.1 μm. Besides, the minimum inclusion size for nucleation is 0.2 μm [20, 21]. Tae-kyu et al. [22] examined low-carbon steel WM and classified the inclusions into two groups of the non-nucleant and the nucleant. Then, by examining the inclusions' size, the researchers concluded that the nucleant inclusions were much larger than the non-nucleant inclusions. Therefore, by increasing the size of the inclusions with a given chemical composition, the normal and sympathetically nucleation of AF increased. In fact, by increasing inclusion size, nucleation of ferritic laths with different crystalline orientations was boosted, which resulted in improved mechanical properties.

There are no general principles about the appropriate amount and proportion of alloying elements in WM and flux. For instance, Mo enhances the steel's hardenability, reduces the penetration, and increases tempering temperatures. It also delays the austenite to pearlite transformation much more than the austenite to bainite transformation; therefore, Mo rich steels can be cooled continuously to produce bainite [23]. On the other hand, Cr usually has a role in enhancing the corrosion and wear resistance, hardness, and high-temperature strength of steels [24]. Bohle et al. [25] examined the effect of Ni, Mo, and Ni-Mo addition on WM of high strength low alloy (HSLA) steels. It was found that adding 1 wt% Mo to WM increases the AF, the tensile strength, and impact toughness. Junhua et al. [26] investigations on Mo's effect on the mechanical and microstructural

properties of HSLA steels in pipelines contradict the Bohle's results. Junhua experiments revealed that increasing Mo would improve UTS and hardness while decreasing the impact toughness.

Despite 100 years of applying arc welding, metallurgists still encounter many problems. Higher-strength WM needs to have higher alloying elements, leading to ductility deterioration along with cold and hydrogen cracking. New generation active fluxes need to be developed to meet the requirement of weldments in service and lower the cost to performance ratio of many steel grades. Reformulating and modeling active fluxes can be a leap towards helping many researchers and industries. Therefore, in this study, the high-quality active fluxes were developed for welding, cladding, and surfacing. Moreover, microstructure, indentation hardness, tensile properties, and impact toughness of specimens welded by these fluxes were thoroughly investigated.

Materials And Methods

The chemical composition of ST37 low carbon steel with the dimensions of 250×120×15 mm^3 as BM and S2 copper-coated 4 mm in diameter as WW with UTS of 450 MPa and 25% Elongation are presented in Table 1.

Commercial OP139 aluminate-basic neutral agglomerated flux with the boniszewski BI of 1.5 with chemical composition listed in Table 2 was supplied by AMA Industrial Company as primary flux. Ferrochromium (FeCr) and ferromolybdenum (FeMo) with the chemical composition shown in Table 3 are used as the alloying powder for producing various active bonded fluxes. The OP139 was ball-milled for two hours to reach the desired uniform particle size (20-50 μm). FeCr, FeMo, and OP139 were mixed with various weight percentages and then ball-milled for 30 minutes. Later on, sodium silicate adhesive (diluted to 80%) was added to various fluxes, air-dried, and baked at 350 °C for 90 minutes. Finally, the active fluxes were crushed and sieved to reach a uniform grain size of 0.3 to 1 mm. Table 4 gives the parameters for all the SAW welds by different fluxes. The groove characteristics for welding by SAW and the bead-on-plate technique are shown in Fig. 1.a. Welding by bead-on-plate technique was performed using the fluxes re-dried for 90 minutes at 150 °C and automotive SAW machine. High-quality weld bead with a penetration shape factor of 2.4 and dilution of 55% are shown in Fig. 1.b. 7 specimens were welded by given parameters and bonded active flux with different amounts of FeMo, FeCr, and FeCr-FeMo powders. The Cr, Mo, Mn composition of the WMs are given in Table 5.

To investigate the welded specimen's microstructure and constituent phases, the weld cross-section was cut from the welded joint to 15×20 mm^2, and its surface was mechanically grinded with different grades of silicon carbide abrasive sandpaper. Then polishing was performed using a solution containing Al_2O_3 particles with a size of 300 and 50 μm followed by 5 μm diamond paste. Finally, the specimens were etched by 2 vol% Nital (2 ml nitric acid and 98 ml ethanol) with 20 seconds dwell time, then gone through hot air drying. The FZ, HAZ, and BM microstructure of each sample were revealed by Olympus PME3 optical microscope. Clemex Image Analysis System and ImageJ software were used to determine the volume fraction of phases. Moreover, a scanning electron microscope (SEM) (TESCAN MIRA3 FEG-SEM) equipped with energy-dispersive X-ray spectroscopy (EDS) detector was used to analyze and measure the distribution and composition of nonmetallic inclusions, slag chemical composition, and fracture mode of impact tests.

The mechanical evaluation comprises Vickers hardness, Charpy V-notch (CVN), and longitudinal tensile test (LTT). The Vickers hardness indentation test using a Bohler instrument (Bohler, Germany) was conducted with a 10 kgF and dwell time of 30 seconds to measure the hardness values of WMs. Samples for LTT, as shown in Fig. 1.a, were prepared along the welding direction from WM according to the standard of ASTM E8M. Tensile tests were performed at ambient temperatures and a constant strain rate of 1.33×10^{-3} s^{-1} with sample gauge length and diameter of 25 and 6 mm, respectively. To determine the room temperature impact toughness, three specimens were prepared for the CVN impact test under the standard of ASTM E23-18 with dimensions of 10×10×55 mm^3 at room temperature. A 2 mm depth and 45° V shape groove with a 0.2 mm notch root radius perpendicular to the welding direction in the center of the welded specimen were machined, as shown in Fig. 1.b. The reported values are the mean results of the three samples.

Results And Discussion

3.1 Microstructural characterization

Fig. 2 signifies the phase fraction of different WMs, and Fig. 3 displays the microstructure of BM, HAZ, and WM welded by neutral agglomerated flux (NAF) and neutral bonded flux (NBF).

The BM microstructure consists of primary allotriomorphic polygonal ferrite (PF) along with a small amount of pearlite (P). The HAZ microstructure is a combination of grain boundary PF and WF. These two expected microstructures are attained according to the weld cooling rate and chemical composition of BM [8]. A similar WM microstructure is achieved for both NAF and NBF, including AF and prior austenite grain boundary ferrite. The amount and type of different ferrite morphologies are approximately equal in both NAF and NBF, which means that the change in the unfused neutral flux manufacturing method does not affect the attained phases and morphologies.

By using the following equation to calculate the percent of element E transferred from flux into WM in SAW [3]:

$$\%E_{WM} = D \cdot \%E_{BM} + (1 - D) \cdot \%E_{WW} + \alpha \cdot \eta_E \cdot \%E_F \qquad \text{(I)}$$

That $\%E_{WM}$, $\%E_{BM}$, $\%E_{WW}$, and $\%E_F$ are the %E in the WM, BM, WW, and active flux, respectively; D, η_E, and α are the dilution, recovery rate of element E and slag factor, respectively. This equation proposed previously by the authors since WW and BM do not have any Cr and Mo, the equation I will be simplified to

$$\%E_{WM} = \alpha \cdot \eta_E \cdot \%E_F \qquad \text{(II)}$$

the slag factor and recovery rate data are calculated and reported in Table 5. This data stated that the recovery rate is reduced whenever using more than one element in the flux. Moreover, by increasing the Mo percentage in the flux, the Mo recovery rate is reduced, but the Cr's recovery rate increased by increasing flux's Cr percentage.

Fig. 4 demonstrates the WM microstructure welded by Cr active bonded fluxes and Mo active bonded fluxes. According to Table 5 and Fig. 2, incorporating 5 wt% FeMo into flux (ABF5Mo) causes the addition of 0.4 wt% Mo into the WM, increases the AF or carbide free bainite formation to 87%, and reduces the PF to 12% by inclusion assisted heterogeneous nucleation. Increasing flux FeMo to 10 wt% (ABF10Mo) causes insertion of 0.7 wt% Mo into WM, 28% bainite formation while decreasing AF fraction to 70% and producing a little amount of grain boundary allotriomorphic ferrite. On the other hand, utilizing 5 wt% FeCr in the flux (ABF5Cr) causes increasing WM's Cr to 0.4 wt% and the formation of 57 vol% AF in the WM. Increasing flux FeCr to 10 wt% (ABF10Cr) cause adding 1.5 wt% Cr into the WM; as the AF decreases to 50 vol%, 46% of the microstructure comprises bainite. Compared to NBF, Cr and Mo addition are found to be quite effective in promoting AF formation. However, AF Vol% decreases by increasing the Cr and Mo content by up to 10 wt%. Moreover, the higher percentage of Cr and Mo caused bainite formation due to the effect of higher alloying elements.

Fig. 5 shows the microstructure of the WMs by simultaneous addition of the different amounts of FeCr and FeMo into the bonded flux. As 1.5 wt% FeCr and 2.5 wt% FeMo (ABF2.5) are added into the flux, 0.2 wt% Cr and 0.2 wt% Mo are transferred into the WM. ABF2.5 microstructure comprises AF morphology predominantly with 83 vol% along with 17% grain boundary allotriomorphic ferrite. By increasing FeCr content to 3 wt% and FeMo to 5 wt% (ABF5), WM's Cr and Mo enhanced to 0.28 wt% and 0.35 wt%, respectively. In ABF5, the AF fraction of microstructure turns to 95 vol%, and the amount of allotriomorphic ferrite is further reduced to 5 vol%, and the whole microstructure morphology changes to favorable AF by the assisting of the proper size and number density of nonmetallic inclusions. Moreover, ferritic laths nucleate on larger inclusions to reduce the larger curvature of the inclusion-ferrite interface [9,27]. Large inclusions foster AF nucleation and are favored by the system, while smaller ones hinder the grain boundary migration and may be engulfed by large laths [6, 29, 30]. By adding 6 wt% FeCr and 10 wt% FeMo into the flux (ABF10), WM's Cr and Mo increases to 0.45 and 0.61 Wt%, respectively. ABF10 samples' AF vol% decreases to 60%, but 38% bainite forms and low strength allotriomorphic ferrite almost disappears. The effect of the

simultaneous addition of Cr and Mo on the formation of AF is far better than the effect of an individual addition of these elements. Increasing FeCr and FeMo causes the reconstructive transformation of allotriomorphic grain boundary ferrite to become sluggish and promotes the displacive transformation of AF and bainite [15, 31].

More rapid cooling rates change the microstructure into acicular ferrite, and further increasing of it results in the emergence of upper bainite with little harmful microphases. Moreover, it is possible to increase the AF Vol% by increasing WM's prior austenite grain size and oxygen content. The oxygen concentration of steel BMs is almost always less than that of the WM's; therefore, oxygen can be a positive boon or a negative bane; it helps to have a higher number density of complicated inclusions while reducing prior austenite grain size and inclusions size [32–34]. Fig. 6 indicates the size and number density of inclusions within different morphologies. Irregular-shaped nonmetallic inclusions comprise a wide variety of oxides and compounds with various crystalline and amorphous phases [9, 22]. These inclusions are favorable sites for stimulation of AF nucleation, and their characteristics have a significant influence on the microstructure. The nature of the inclusions varies by the chemical composition of the WM. ABF5 comprises moderate inclusion number density with 95 vol% acicular ferrite, demonstrating that high inclusion number density does not necessarily cause a higher vol% of AF. Additionally, the proper inclusion size range is necessary for AF nucleation since larger ones deteriorate mechanical properties, whereas the smaller ones are engulfed by ferritic laths.

Fig. 7 reveals the EDS point scan chemical analysis of inclusions in different WMs. Oxygen content, cooling rate, alloying elements, BI, and prior austenite grain size affect the inclusion size and composition, which later manipulate the AF vol%. Inclusions have 10-15 wt% oxygen in their analysis, and according to the results, by the addition of FeCr and FeMo into the flux, Mo and Cr rich nonmetallic inclusions are formed, promoting AF nucleation. The following conditions increase the nucleation of AF fostered by inclusions: 1. Slight lattice strain misfit between the inclusions and matrix, 2. The positive thermal strain around inclusions due to the significant difference in coefficient of thermal expansion (CTE) with matrix, 3. The minimization of the interface energy, and 4. forming manganese free zone around the MnS included inclusions [23, 29]. Fig. 8 shows the results of the EDS point scan analysis of the ABF5 slag. According to the results, by adding FeCr and FeMo into the flux, 0.37 wt% Mo and 0.03 wt% Cr are lost from flux into the slag, emphasizing the role of elements recovery rate in active fluxes. Elements have different recovery rates and are affected by the presence of other elements. In addition, the Mn in the slag is 3.23 wt% by considering the slag to the WM ratio, which is a significant loss.

3.2 Tensile and indentation hardness evaluation

Fig. 9 represents the mechanical properties of the WMs, including the results of the LTT and Vickers hardness indentation test. The tensile and hardness values of the WM-NBF and WM-ABF are almost the same and higher than that of BM owing to AF's formation without jeopardizing the toughness. The ABF5Mo enhances the hardness value of the WM's, improves the UTS, reduces the ductility slightly, and increases the strength due to the solid solution mechanism of alloying elements and acicular ferrite formation with high dislocation density [35–37]. Further increasing in WM's Mo content, ABF10Mo causes increasing in UTS, YS, and hardness, but elongation reduced by 50% compared to NBF. AF and the formation of bainite are the main reason behind these changes.

On the other hand, ABF5Cr increases UTS to 554 MPa and reduces the ductility by 23%. The UTS and hardness value of ABF10Cr are improved by 73% and 11%, respectively, but the elongation decreases sharply by 67% because of the reduction of AF vol% and increase of bainite. Microphases and morphologies rather than AF are detrimental to WM toughness since crack can propagate quickly through the matrix.

ABF2.5 YS, UTS, and HV improve by 28%, 17%, and 3%, while elongation decreases by 24%. ABF2.5's AF vol% increases to 83%, enhancing the UTS. Moreover, ABF5's YS, UTS, and HV increase by 37%, 23%, and 9%, while elongation decreases by 39% due to the high Vol% of AF of 97%. Finally, ABF10 YS, UTS, and HV rise by 56%, 35%, and 5%, respectively, but due to reducing the AF to 60% and the 38 vol% bainite formation, elongation is reduced slightly by 38%. It is found that by increasing alloying elements, hardenability increases due to the high WM's CE, which causes the formation of bainite and an increase in UTS. The

high percentage of AF, approximately higher than 70%, does not have an enormous effect on tensile properties, while the generation of bainite further increases the UTS by scarifying the elongation.

It seems that at least 50% AF, along with WF and allotriomorphic ferrite, is acceptable. On the other hand, mechanical properties can be discussed by considering the effect of nonmetallic inclusions. They also play a critical role in the toughness; hard and brittle inclusions, along with large size, promote crack nucleation and propagation through grain boundary allotriomorphic ferrite [7, 11, 13]. Therefore, optimum inclusion size and density number, which have good lattice matching with the matrix, stimulate sheaves of heterogeneously AF formation, deflecting and hindering crack propagation and arresting the cracks to maximize the toughness.

3.3 Impact toughness and fractography

The results of the CVN impact test of different WMs are presented in Fig. 9. The WM's impact toughness of NAF and NBF is 144 and 146 J, respectively, so changing the unfused welding flux's production method has almost no effect on the impact toughness. Compared to BM, the impact toughness of the NAF and NBF are sharply boosted by 440%.

By adding alloying elements into the flux, the impact toughness of the WMs is reduced. The result is still controversial, being both in agreement and contradiction with literature. Different BM, types, and amounts of alloying elements in the WM, welding parameters, impurities inserted in the WM by the welding flux, and different amounts of hydrogen, nitrogen, oxygen, sulfur, and phosphorus in the WM are the main reasons for the controversial results. The impact toughness of all the alloyed WMs is compared with NBF. ABF5Mo and ABF10Mo both have induced a 28% reduction in the impact toughness due to the presence of inclusions and detriment microphases. As a result, the impact toughness has experienced a slight decrease.

On the other hand, ABF5Cr impact toughness significantly decreases by 36%. By further Cr increasing, ABF10Cr impact toughness is reduced abruptly by 59% to 60 J. Both ABF10Mo and ABF10Cr comprise bainite, which includes Fe_3C among ferrite phases, and the nature of cementite should be considered, as well.

ABF2.5 and ABF5 have the same impact toughness of about 115 J; however, their impact toughness is 21% lower than that of NBF. As Mo and Cr are further increased, the amount of AF decreases, which along with bainite formation, results in a 33% decrease in impact toughness. Therefore, optimum WM tensile toughness and impact toughness are achieved through a higher vol% of AF.

Fig. 10 shows the fracture surface of different WMs through the CVN impact test. All samples' fracture mode is a combination of ductile and brittle. NBF comprises regular and elongated dimples and voids with a considerable amount of shear facets. ABF5Mo includes deeper dimples with embedded inclusions. ABF5Cr impact toughness is 93 J and incorporates higher inclusions size with a large fraction of shear facets and shallow dimples, harmful to toughness. A higher density of inclusions on the fracture surface is observed in ABF5. ABF5 has the impact toughness of 113 J; it also comprises voids and debonded particles, indicating voids nucleation and coalescence, which later give rise to crack formation [38, 39].

Conclusion

In this study, the bonded unfused method was used to manufacture active welding fluxes by incorporating the different amounts of Cr and Mo to basic neutral agglomerated OP139 flux. The submerged arc welding (SAW) by the bead-on-plate technique with the manufactured fluxes was used to implement a weld pass on ST37 low carbon steel. The following results were obtained:

- The microstructure, tensile properties, and impact toughness of WMs' achieved by bonded and agglomerated neutral unfused fluxes were almost the same. Moreover, alloying elements were added to the bonded fluxes without adversely affecting the welding flux's functions, such as protecting and purifying the weld puddle.

- The largest vol% of acicular ferrite (95%) was formed by incorporating 5% FeMo and 3% FeCr in the flux. Besides, the size and number density of nonmetallic irregular inclusions had a significant effect on the heterogenous intragranular nucleation and growth of the sympathetic or autocatalytic acicular ferrite laths. The mean size and number density of inclusions obtained from Mo fluxes' are more than Cr fluxes.
- While adding 5% FeCr into flux (ABF5Cr) caused a 57% formation of acicular ferrite in WM microstructure, 5% FeMo resulted in an 87% acicular ferrite formation. Additionally, FeCr flux increased UTS intensely and decreased the impact toughness and elongation sharply. Furthermore, each element's recovery rate and slag to WM ratio determine the amount of element transferred from flux into WM.
- Incorporating Cr-Mo in the WM caused a higher vol% of acicular ferrite than each element's individual addition. Averagely, 1 mm^2 of WM's microstructure produced by the 0.35% Mo-0.28% Cr flux comprised 73 inclusions with a mean size of 1.1 mm and 95% acicular ferrite. The constant increase of WM's Cr-Mo continuously enhanced UTS and HV, whereas declined elongation and impact toughness. Therefore, 10% FeMo and 6% FeCr (ABF10) improved UTS and HV of neutral bonded flux by 35% and 11%, respectively; while, brought about a 33% lower impact toughness and a 38% lesser elongation.

Declarations

The authors have no financial or proprietary interests in any material discussed in this article.

- **Ethical Approval:** not applicable

- **Consent to Participate:** The authors have no financial or proprietary interests in any material discussed in this article.

- **Consent to Publish :** The figure(s)/table(s) submitted have not been published before or are in the public domain. We consent to publish this paper in your journal.

- **Funding:** No funds, grants, or other support was received.

- **Competing Interests:** The authors declare that they have no known competing financial interests or personal relationships that could have appeared to influence the work reported in this paper.

- **Availability of data and materials:** (Do not apply) not applicable.

Acknowledgements

All persons who have made substantial contributions to the work reported in the manuscript (e.g., technical help, writing and editing assistance, general support), but who do not meet the criteria for authorship, are named in the Acknowledgements and have given us their written permission to be named. If we have not included an Acknowledgements, then that indicates that we have not received substantial contributions from non-authors.

References

1. Sharma SK, Maheshwari S (2017) A review on welding of high strength oil and gas pipeline steels. J Nat Gas Sci Eng 38:203–217. https://doi.org/10.1016/j.jngse.2016.12.039
2. Bose-Filho WW, Carvalho ALM, Strangwood M (2007) Effects of alloying elements on the microstructure and inclusion formation in HSLA multipass welds. Mater Charact 58:29–39. https://doi.org/10.1016/j.matchar.2006.03.004
3. Alishavandi M, Mohammadmirzaei M, Ebadi M, Kokabi AH (2020) Microstructural and mechanical evaluation of submerged arc welded HSLA 4135 steel by modeled and manufactured granular Cr-Mo bonded active basic flux. J Mater Process Technol 116890. https://doi.org/https://doi.org/10.1016/j.jmatprotec.2020.116890
4. Sirin K, Sirin SY, Kaluc E (2016) Influence of the chemical composition of weld electrode on the mechanical properties of submerged arc welded pipe. Int J Adv Manuf Technol 87:1941–1950. https://doi.org/10.1007/s00170-016-8546-z

5. Chen X wei, Qiao G ying, Han X lin, et al (2014) Effects of Mo, Cr and Nb on microstructure and mechanical properties of heat affected zone for Nb-bearing X80 pipeline steels. Mater Des 53:888–901. https://doi.org/10.1016/j.matdes.2013.07.037
6. Luo J, Dong Y, Li L, Wang X (2014) Microstructure of 2205 duplex stainless steel joint in submerged arc welding by post weld heat treatment. J Manuf Process 16:144–148. https://doi.org/https://doi.org/10.1016/j.jmapro.2013.06.013
7. Yadav A, Ghosh A, Kumar A (2017) Experimental and numerical study of thermal field and weld bead characteristics in submerged arc welded plate. J Mater Process Technol 248:262–274. https://doi.org/https://doi.org/10.1016/j.jmatprotec.2017.05.021
8. Kou S (2002) Welding Metallurgy. John Wiley & Sons, Inc.
9. Lan L, Kong X, Qiu C, Zhao D (2016) Influence of microstructural aspects on impact toughness of multi-pass submerged arc welded HSLA steel joints. Mater Des 90:488–498. https://doi.org/https://doi.org/10.1016/j.matdes.2015.10.158
10. Lippold JC (2014) Welding Metallurgy and Weldability. John Wiley & Sons, Inc
11. Thewlis G (2000) Weldability of X100 linepipe. Sci Technol Weld Join 5:365–377. https://doi.org/10.1179/136217100101538434
12. Beidokhti B, Koukabi AH, Dolati A (2009) Effect of titanium addition on the microstructure and inclusion formation in submerged arc welded HSLA pipeline steel. J Mater Process Technol 209:4027–4035. https://doi.org/10.1016/j.jmatprotec.2008.09.021
13. Huda N, Gianetto J, Ding Y, et al (2019) Investigation of local tensile strength and ductility properties of an X100 submerged arc seam weld. Mater Sci Eng A 768:138475. https://doi.org/10.1016/j.msea.2019.138475
14. Sakamoto R, Kobayashi K, Iijima T, Mizo Y (2012) Development of Submerged arc Welding Method in a Vertical Upward Position. Weld World 56:64–71. https://doi.org/10.1007/BF03321366
15. Mohammadijoo M, Collins L, Lazor R, et al (2018) Influence of cold-wire submerged arc welding on the toughness of microalloyed steel. Weld J 97:338S-352S. https://doi.org/10.29391/2018.97.029
16. Haslberger P, Ernst W, Schnitzer R (2017) High resolution imaging of martensitic all-weld metal. Sci Technol Weld Join 22:336–342. https://doi.org/10.1080/13621718.2016.1240980
17. Zhang S, Melfi T, Narayanan BK (2016) Effects of precipitates on mechanical properties of P91 submerged arc welds. Sci Technol Weld Join 21:147–156. https://doi.org/10.1179/1362171815Y.0000000076
18. da Silva MM, Batista VR, Maciel TM, et al (2018) Optimization of submerged arc welding process parameters for overlay welding. Weld Int 32:122–129. https://doi.org/10.1080/09507116.2017.1347325
19. Thewlis G (1994) Transformation kinetics of ferrous weld metals. Mater Sci Technol (United Kingdom) 10:110–125. https://doi.org/10.1179/mst.1994.10.2.110
20. Lu Y, Chen J, Zhang Y, Kvidahl L (2014) Predictive control based double-electrode submerged arc welding for filet joints. J Manuf Process 16:415–426. https://doi.org/https://doi.org/10.1016/j.jmapro.2014.05.001
21. Sengupta V, Havrylov D, Mendez PF (2019) Physical phenomena in the weld zone of submerged arc welding - A review. Weld J 98:283S-313S
22. Sarma DS, Karasev A V., Jönsson PG (2009) On the role of non-metallic inclusions in the nucleation of acicular ferrite in steels. ISIJ Int 49:1063–1074. https://doi.org/10.2355/isijinternational.49.1063
23. Bhadeshia H, Honeycombe R (2017) Chapter 13 - Weld Microstructures. In: Bhadeshia H, Honeycombe R (eds) Steels: Microstructure and Properties (Fourth Edition), Fourth Edi. Butterworth-Heinemann, pp 377–400
24. Ishigami A, Roy MJ, Walsh JN, Withers PJ (2017) The effect of the weld fusion zone shape on residual stress in submerged arc welding. Int J Adv Manuf Technol 90:3451–3464. https://doi.org/10.1007/s00170-016-9542-z
25. Bhole SD, Nemade JB, Collins L, Liu C (2006) Effect of nickel and molybdenum additions on weld metal toughness in a submerged arc welded HSLA line-pipe steel. J Mater Process Tech 173:92–100. https://doi.org/10.1016/j.jmatprotec.2005.10.028

26. Junhua K, Lin Z, Bin G, et al (2004) Influence of Mo content on microstructure and mechanical properties of high strength pipeline steel. Mater Des 25:723–728. https://doi.org/10.1016/j.matdes.2004.03.009
27. Suman S, Biswas P (2020) Comparative study on SAW welding induced distortion and residual stresses of CSEF steel considering solid state phase transformation and preheating. J Manuf Process 51:19–30. https://doi.org/https://doi.org/10.1016/j.jmapro.2020.01.012
28. Reisgen U, Schäfer J, Willms K (2016) Analysis of the submerged arc in comparison between a pulsed and non-pulsed process. Weld World 60:703–711. https://doi.org/10.1007/s40194-016-0336-6
29. Bhadeshia H, Honeycombe R (2017) Chapter 7 - Acicular Ferrite. In: Bhadeshia H, Honeycombe R (eds) Steels: Microstructure and Properties (Fourth Edition), Fourth Edi. Butterworth-Heinemann, pp 203–216
30. Tsuyama T, Nakai K, Tsuji T (2014) Development of submerged arc welding method using hot wire. Weld World 58:713–718. https://doi.org/10.1007/s40194-014-0153-8
31. Mortazavian E, Wang Z, Teng H (2020) Repair of light rail track through restoration of the worn part of the railhead using submerged arc welding process. Int J Adv Manuf Technol 107:3315–3332. https://doi.org/10.1007/s00170-020-05208-x
32. Pratap Singh R, Singh A, Singh A (2020) Optimization of hardness of weld in submerged arc welding. Mater Today Proc. https://doi.org/10.1016/j.matpr.2020.02.382
33. Aleshin NP, Grigor'ev M V, Kobernik N V, et al (2019) Erratum to: Modification of Weld Metal with Tungsten Carbide and Titanium Nitride Nanoparticles in Twin Submerged Arc Welding. High Energy Chem 53:176. https://doi.org/10.1134/S0018143919090017
34. Osorio AG, Souza D, dos Passos T, et al (2019) Effect of niobium addition on the flux of submerged arc welding of low carbon steels. J Mater Process Technol 266:46–51. https://doi.org/https://doi.org/10.1016/j.jmatprotec.2018.10.020
35. Koseki T (2005) A review on inclusion-assisted microstructure control in C-Mn and low-alloy steel welds. Weld World 49:22–28. https://doi.org/10.1007/BF03263406
36. Li XR, Zhang YM, Kvidahl L (2013) Penetration depth monitoring and control in submerged arc welding. Weld J 92:48–56
37. Lu Y, Zhang YM, Kvidahl L (2013) Heat input reduction in fillet welding using bypass and root opening. Weld J 92:
38. Mohammadijoo M, Collins L, Henein H, Ivey DG (2017) Evaluation of cold wire addition effect on heat input and productivity of tandem submerged arc welding for low-carbon microalloyed steels. Int J Adv Manuf Technol 92:817–829. https://doi.org/10.1007/s00170-017-0150-3
39. Liu L, Chen M, Li C, Yang L (2014) A new superimposed double-arc welding method with one arc submerged in the weld pool. Int J Adv Manuf Technol 75:331–337. https://doi.org/10.1007/s00170-014-6116-9

Tables

Table 1 Chemical composition and carbon equivalent of the BM and the WW (wt%).

Code	Standard	Grade	Fe	C	Mo	Cr	Mn	Si	S	P	CE_{AWS}
BM	**DIN 2391**	**ST37**	balanced	0.23	ND	0.20	0.90	0.50	0.002	0.02	0.503
WW	**DIN 8557**	**S2**	balanced	0.07	ND	ND	1.10	0.10	ND	ND	ND

Table 2 Compositions of the neutral agglomerated flux (wt%).

Flux	Standard	Grade	SiO_2+TiO_2	CaO+MgO	Al_2O_3+MnO	CaF_2
OP139	DIN 32522	B AB 1 67 AC 12 MHP5	20%	25%	35%	15%

Table 3 The composition of active powders (wt%).

Powder	Cr	Mo	Fe	C
Ferrochromium (FeCr)	**75**	**ND**	**24.7**	**0.3**
Ferromolybdenum (FeMo)	**ND**	**45**	**54.9**	**0.1**

Table 4 The SAW main parameters.

Current (A)	Voltage (V)	Speed (mm/s)	Heat Input (KJ/mm)	Stick out (mm)	Welding Wire Diameter (mm)	Number of Pass	Polarity	Number of Wire	Wire Angle	Deposition rate (Kg/h)
500	**29**	**4**	**3.625**	**28**	**4**	**1**	**DCEP**	**single**	**Vertical**	**6.6**

Table 5 Chemical composition, recovery rate, slag factor, and dilution of different WMs.

Code	Flux	Mn	Cr	Mo	ηCr	ηMo	α	%D
NAF	OP139	1.06	-	-	-	-	0.41	55
NBF	OP139	1.10	-	-	-	-	0.38	62
ABF5Mo	OP139-5%FeMo	1.13	-	0.40	-	0.46	0.39	48
ABF10Mo	OP139-10%FeMo	1.05	-	0.71	-	0.38	0.42	52
ABF5Cr	OP139-5%FeCr	1.08	0.4	-	0.34	-	0.31	50
ABF10Cr	OP139-10%FeCr	1.10	1.53	-	0.55	-	0.37	52
ABF2.5	OP139-2.5%FeMo-1.5%FeCr	1.03	0.20	0.20	0.38	0.38	0.47	65
ABF5	OP139-5%FeMo-3%FeCr	1.00	0.28	0.35	0.29	0.36	0.43	59
ABF10	OP139-10%FeMo-6%FeCr	1.06	0.45	0.61	0.27	0.37	0.37	60

Figures

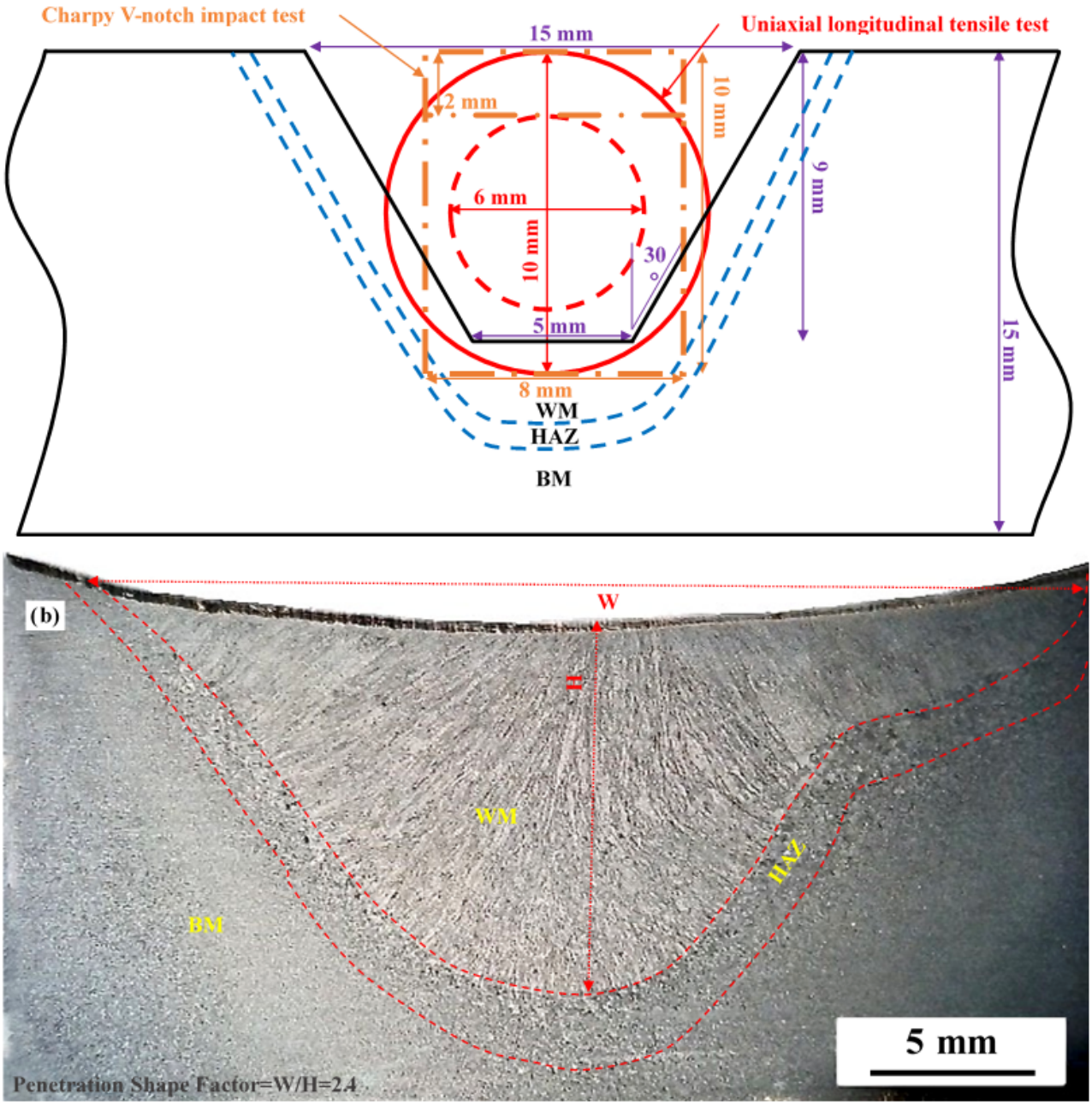

Figure 1

Weld metal cross section: (a) groove characteristics and extracted position of tensile and CVN samples, (b) bead-on-plate welding by active bonded flux.

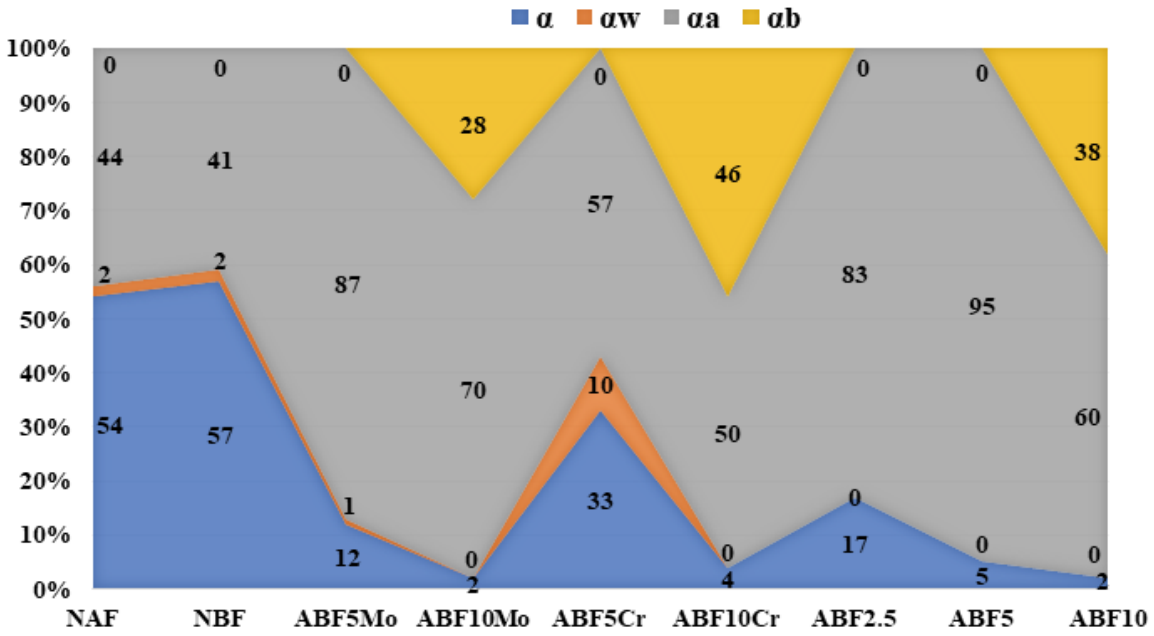

Figure 2

Volume percent (vol%) phases fraction of different WMs.

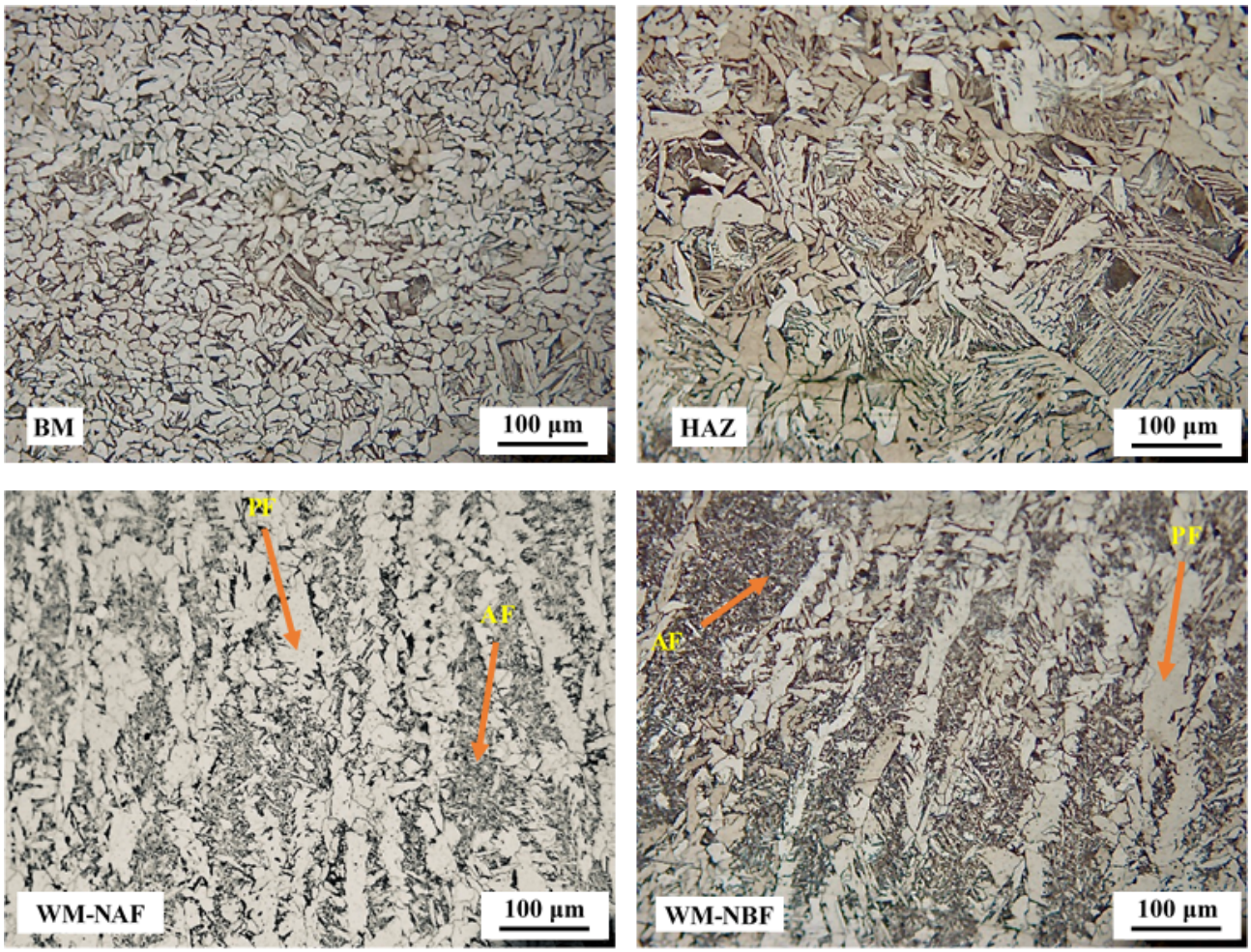

Figure 3

Optical microscopy of: (a) base metal, (b) heat affected zone, (c) weld metal welded by neutral agglomerated flux, and (d) weld metal welded by neutral bonded flux.

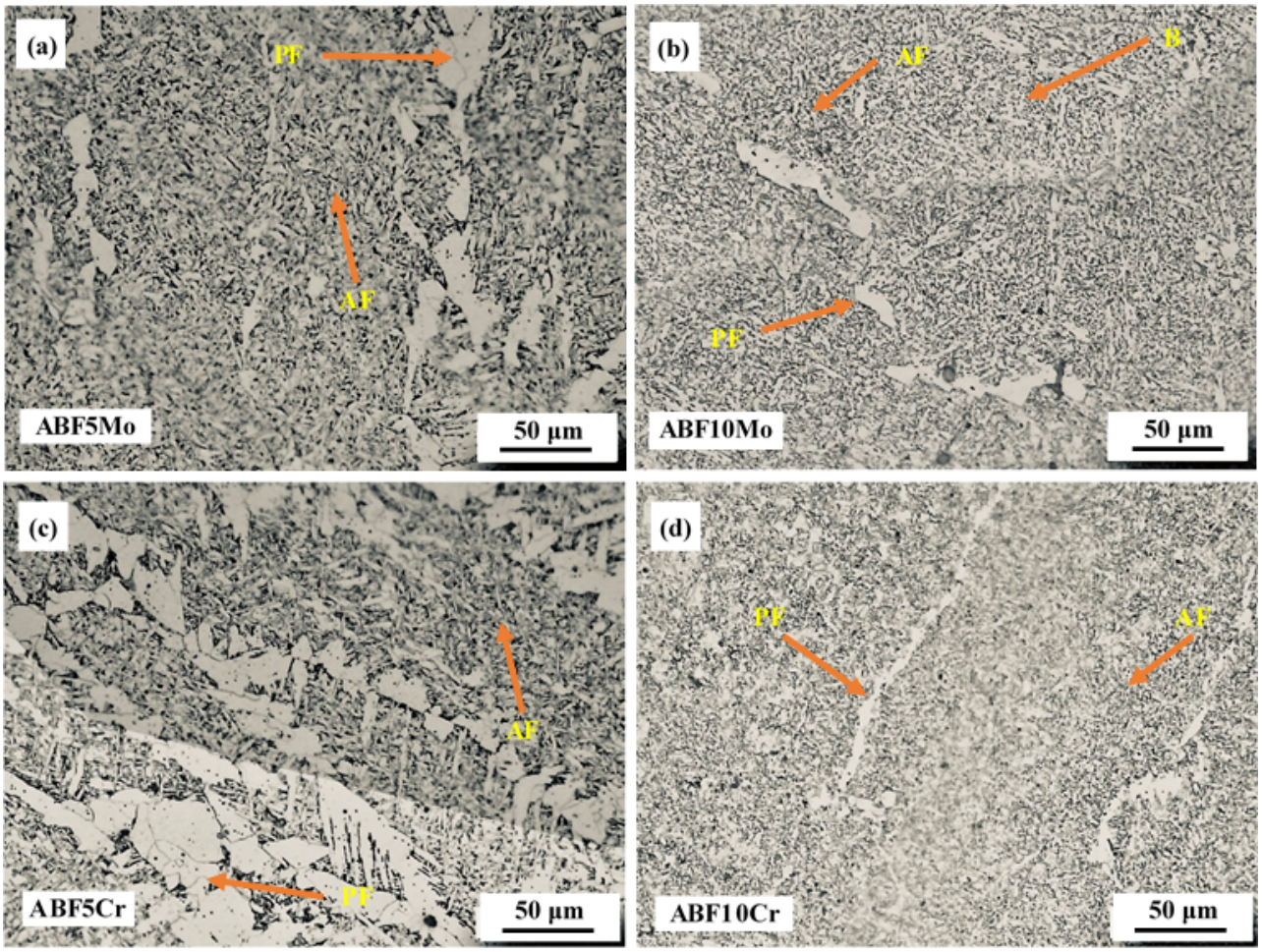

Figure 4

Optical microscopy of WMs by active bonded flux with: (a) 5 %wt FeMo, (b) 10 %wt FeMo, (c) 5 %wt FeCr, (d) 10 %wt FeMo.

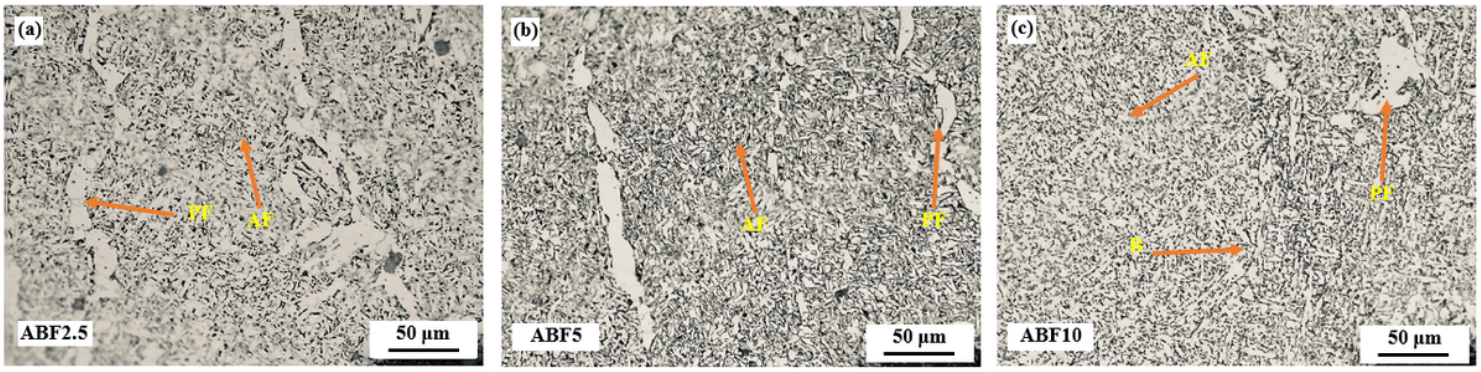

Figure 5

Optical microscopy of WMs by active bonded flux with: (a) 2.5 %wt Mo and 2.5%wt Cr, (b)) 2.5 %wt Mo and 2.5 %wt Cr, (c) 5 %wt Cr and 5 %wt Mo.

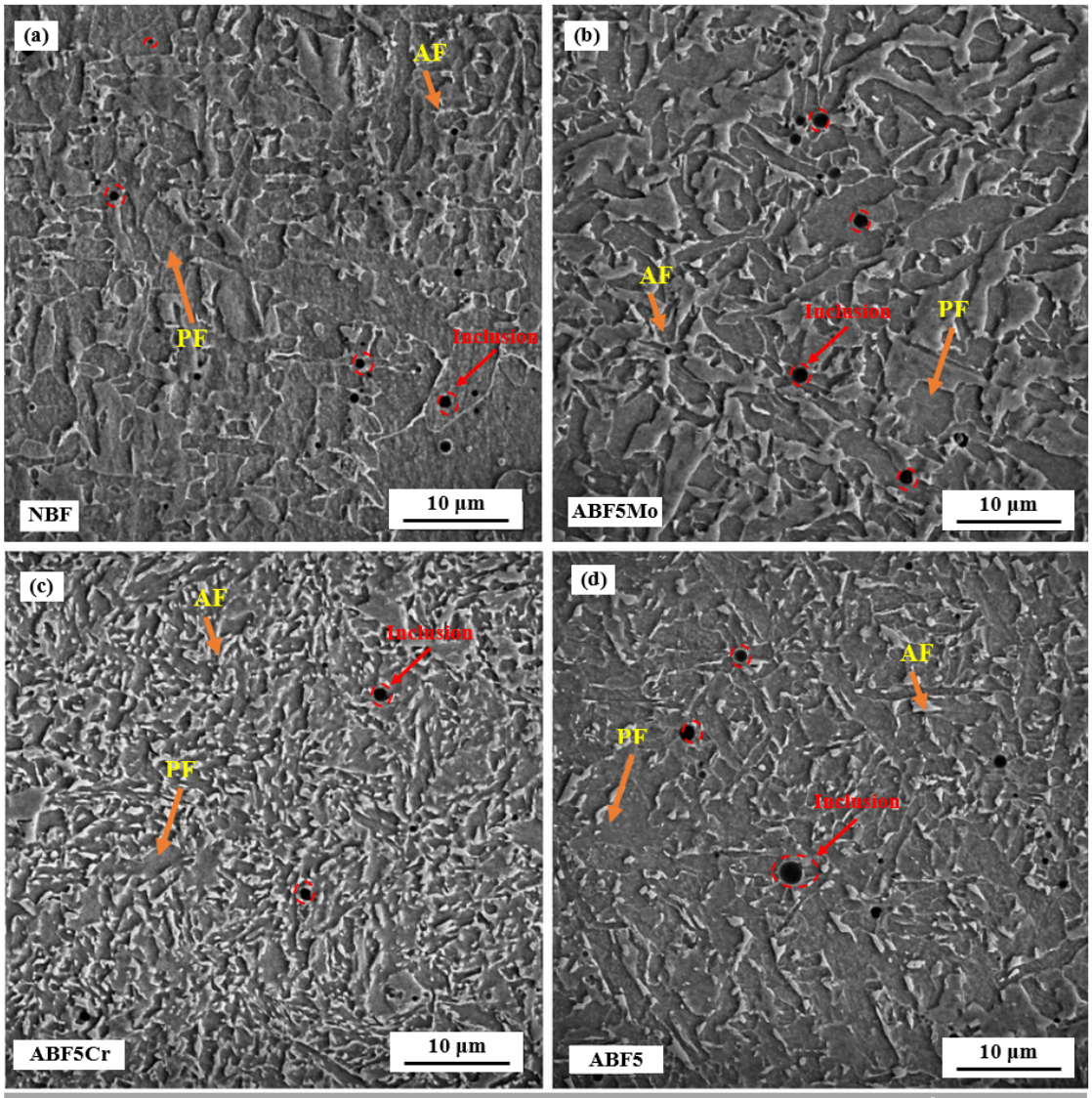

	Inclusion Diameter (µm)	Inclusion Count in 1mm^2
NBF	0.5 – 1.3	120-160
ABF5Mo	0.6 – 1.7	48-72
ABF5Cr	0.4 – 1.1	28-44
ABF5	0.5 – 1.7	56-80

Figure 6

SEM images of inclusions and size-number and their effect on the heterogenous nucleation of acicular ferrite laths of as-welded WMs by: (a) neutral bonded flux, (b) active bonded flux with 5 wt% Mo, (c) active bonded flux with 5 wt% Cr, (d) active bonded flux with 5 wt% Mo and 5 %wt Cr.

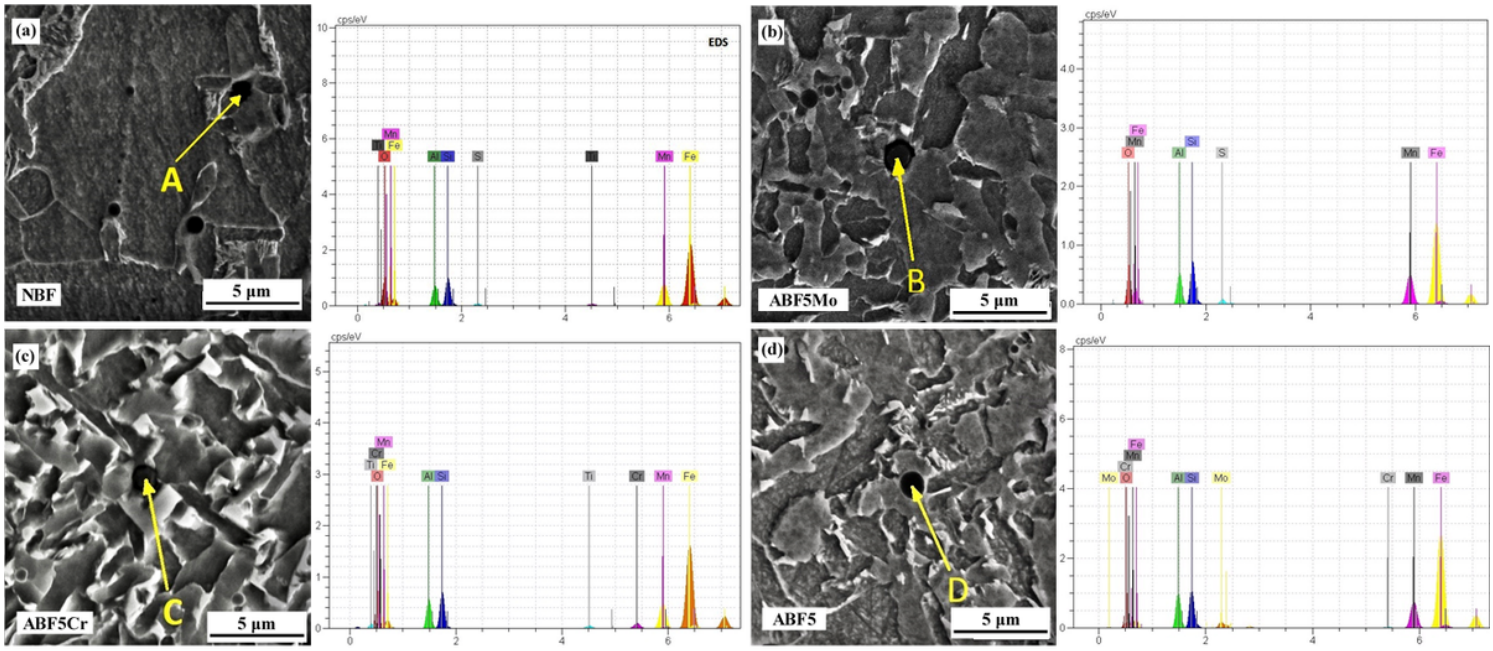

Code	Fe	Mo	Cr	Mn	S	Si	Al	O
NBF	53.54	ND	ND	13.77	0.51	10.35	9.00	12.83
ABF5Mo	51.07	2.70	ND	14.23	1.11	8.40	7.09	15.40
ABF5Cr	54.65	ND	1.72	12.92	ND	8.83	9.02	12.86
ABF5	53.64	3.02	0.28	11.31	ND	10.31	12.21	9.23

Figure 7

EDS point analysis, size and number of inclusions: (a) neutral bonded flux, (b) active bonded flux with 5 wt% Mo, (c) active bonded flux with 5 wt% Cr, (d) active bonded flux with 5 wt% Mo and 5 %wt Cr.

Point A	O	Mg	Ca	Si	Al	Mn	Na	N	Fe	K	Ti	Mo	Cr
Wt%	46.75	13.07	12.16	10.19	6.33	3.23	3.04	1.81	1.14	1.08	0.80	0.37	0.03

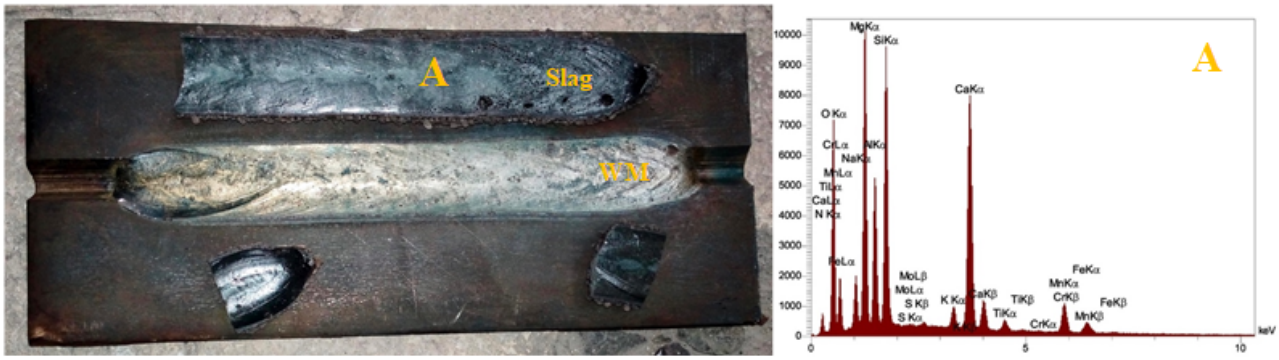

Figure 8

Slag EDS analysis of ABF5 sample.

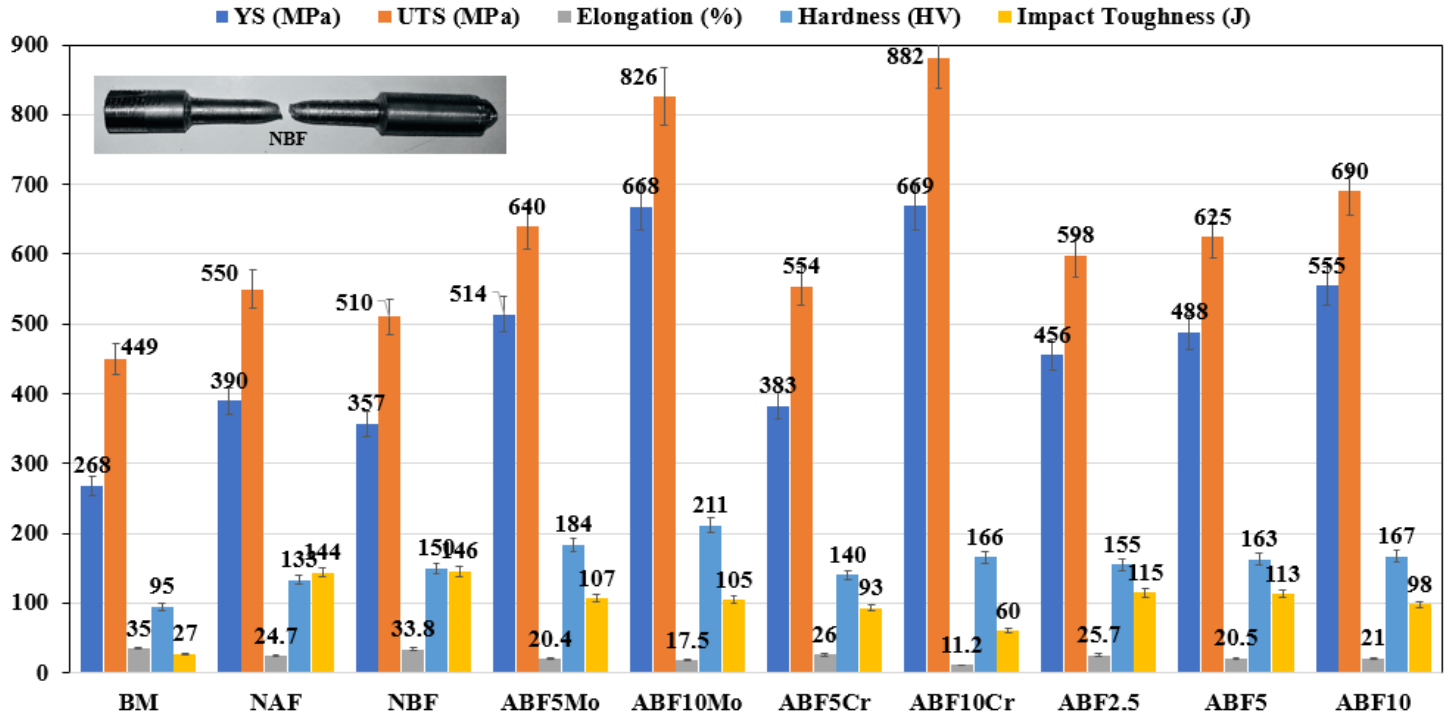

Figure 9

Main tensile properties, Vickers hardness, and impact absorbed energy of the examined samples.

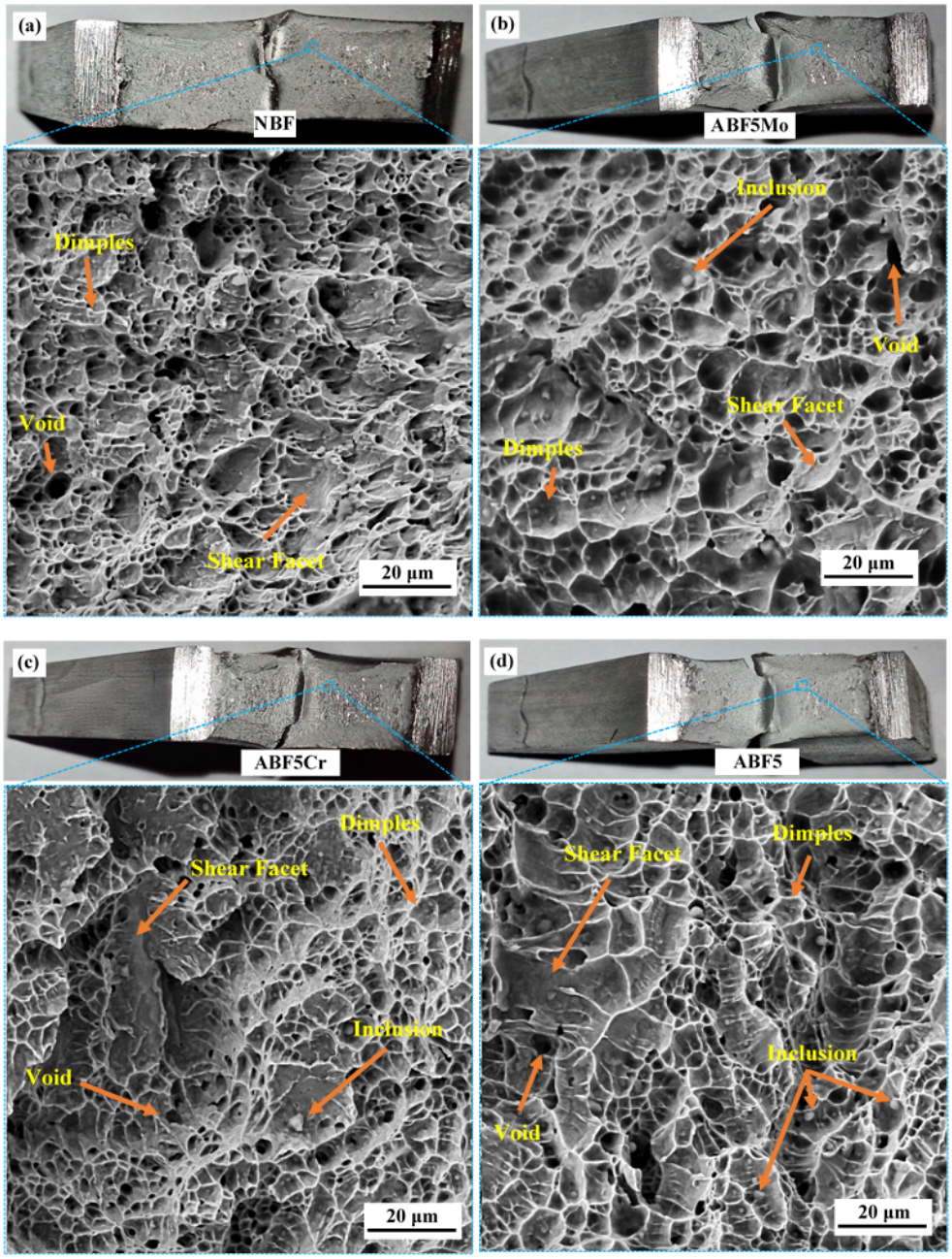

Figure 10

SEM images showing fracture appearances of impact test as-welded WM welded by: (a) neutral bonded flux, (b) active bonded flux 5%wt Mo, (c) active bonded flux 5%wt Cr, (d) active bonded flux 5%wt Mo and 5 %wt Cr.

Supplementary Files

This is a list of supplementary files associated with this preprint. Click to download.

- Highlights.docx
- GraphicalAbstract.pdf